Seismic behavior of a piled raft foundation with grid-form DMWs considering post-peak softening of stabilized soil

Yoshimasa Shigeno[1] and K. Yamashita[1]

[1] Research & Development Institute, Takenaka Corporation, Inzai, Chiba, 1-5-1, 270-1395, Japan.

ABSTRACT

The seismic performance of a piled raft foundation with grid-form deep mixing walls (DMWs) in soft ground under strong earthquake loads is numerically evaluated in this study. A base-isolated 12-story building located in Tokyo is modeled in a detailed 3D finite element SSI model. For the constitutive model of stabilized soil, the elasto-plastic model that is able to evaluate shear failure, tension failure and post-peak tension-softening is used. Based on the analysis, it is found that even though the induced stress in the DMWs reaches the tensile strength and the softening occurs, the grid-form DMWs are quite effective at reducing the bending moment of the piles to an acceptable level.

Keywords: piled raft foundation; deep mixing walls; post-peak softening; soil and structure interaction analysis

1 INTRODUCTION

In recent years, piled raft foundations have been used even for liquefiable sand with grid-form cement deep mixing walls (DMWs) (Yamashita et al. 2016). The grid-form DMWs work as a countermeasure for liquefaction, and they also work as a part of foundation. However seismic behavior of this foundation is not well known because of its complexity. Seismic behavior of this foundation has been studied using the seismic observation records and the numerical simulation of the building in Tokyo (Yamashita et al. 2012, Shigeno et al. 2017). And the soundness of the piles was confirmed even though the grid-form DMWs were partially failed by tension under strong earthquake (Yamashita et al. 2018). However, softening of the DMWs after the failure was not considered in the analysis and then the results might be somewhat optimistic.

In this study, the after-peak softening of the stabilized soil is considered using the elasto-plastic model that has the shear and tensile criteria, and also is able to model the softening. The influence of the softening of the DMWs caused by the strong motion on the sectional force of the piles is mainly discussed.

2 OVERVIEW OF THE BUILDING AND GROUND

Figure 1 shows a schematic view of the building and foundation. The building is the 12-story apartment in Tokyo. The height is 38.7m, and the cross section is 33.25 m by 30.05 m. The building is a reinforced concrete structure with a seismic base-isolation system.

The soil down to GL -44 m is alluvial stratum. The upper 7m is fill, soft silt and loose silty sand. The rest is very soft to medium silty clay. The stratum deeper than 44 m is diluvial sand and a gravel layer with SPT N-value of 60 or higher. The ground water table is GL -1.8 m. The building is supported by a piled raft with grid-form DMWs. The spacing between the DMWs is about 6 to 9 m, and the area replacement ratio is 25%.

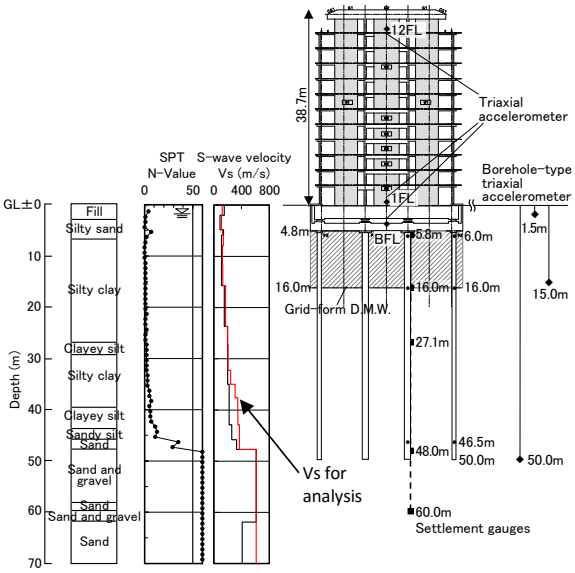

Fig. 1. Cross section of building and foundation with soil profile.

3 ANALYSIS MODEL

3.1 Analysis condition

Figure 2 shows the FE mesh, which has 213,622 elements. The superstructure and the piles were modeled by elastic bars and shells. The material properties of the piles are reported in Shigeno et al. (2017). The raft was modeled by elastic solid elements. Rayleigh damping was applied to these components at a

damping ratio of 2%. Figure 3 shows a top view of the FE mesh beneath the raft. The base isolation system was modeled by a tri-linear spring. The lateral boundaries were periodic boundaries. The bottom was a viscous boundary. The software is the in-house program called MuDIAN (Shiomi et al. 1998).

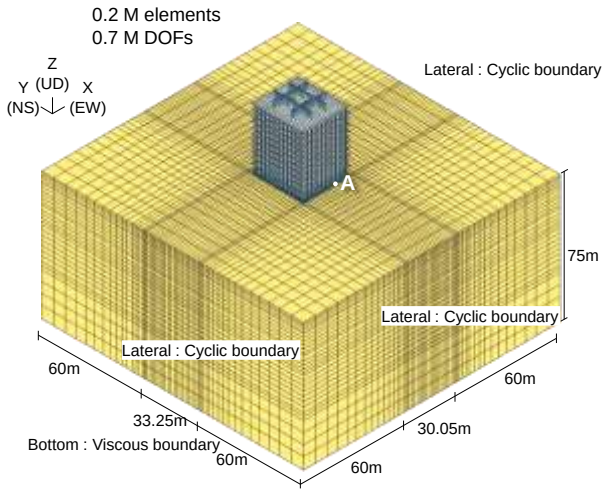

Fig. 2. FE mesh of the soil-structure interaction model.

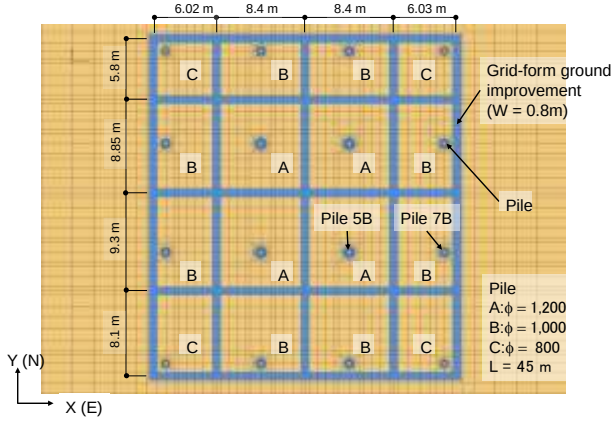

Fig. 3. Magnified top view of FE mesh under the raft.

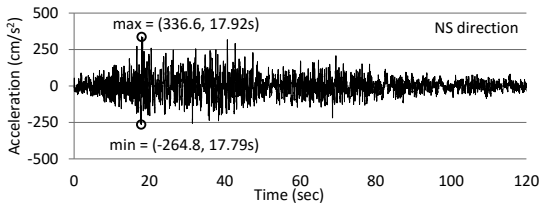

Fig. 4. Input acceleration wave(2E) of Hachinohe phase.

An artificial wave was used for a strong earthquake called 'Level 2 earthquake' that is officially notified in Japanese building design code. The wave is defined by the acceleration response spectrum of which peak is 800 cm/s^2 from 0.16 s to 0.64 s. The Hachinohe phase data at the Tokachi Oki Earthquake (1968) was used to generate the input wave. The NS directional input motion was applied. Figure 4 shows the input motion, and the maximum acceleration is 337 gal.

3.2 Constitutive models

The Yoshida model for multi-dimension (Tsujino et. al., 1994) was used as the constitutive model of the soil. The soil properties are reported in Shigeno et al. (2017).

In the previous study, the importance of considering the tensile criterion for stabilized soil was shown (Yamashita et. al., 2018). However, softening after failure was not considered. In this study, the elasto-plastic model proposed by Namikawa et al. (2007) that has tensile and shear criteria and also be able to evaluate post-peak softening was applied.

For post-peak tension softening, Namikawa assumes the distributed cracks model and the damage function with the fracture energy as a parameter. The damage parameter ω specifying the reduction rate of the tensile strength is expressed as the function of the maximum plastic principal strain ε_1^p (note that tension is positive) using 1/4 bilinear model as follows.

$$\omega = l_m \frac{T_f}{G_f}\left(\varepsilon_1^p - \varepsilon_{1peak}^p\right) \quad \omega \le 0.75$$
$$\omega = \frac{12}{17} - \frac{1}{17} l_m \frac{T_f}{G_f}\left(\varepsilon_1^p - \varepsilon_{1peak}^p\right) \quad 0.75 < \omega \le 1.0 \tag{1}$$

Where, G_f is fracture energy, $\varepsilon_1{}^p{}_{peak}$ is the peak plastic principal strain and l_m is the mesh size dependent parameter.

The Mohr–Coulomb criterion is used for shear. The damage parameter ω for shear failure was obtained from the plane strain compression test and modeled as follows by Namikawa (2006).

$$\omega = 1 - \exp\left\{-\frac{R_l\left(\bar{\varepsilon}^p - \bar{\varepsilon}_{peak}^p\right)}{e_r}\right\} \qquad R_l = \frac{l_m}{l_c} \tag{2}$$

Where, l_c is the characteristic length that specifies the size of the failure region, and e_r is the parameter. The damage parameter ω is the common for both the tensile and the shear criterion, and the both criterion reduce after stress reaches the strength.

The design standard compressive strength F_c and other properties were determined by referring to the proposal of BCJ (2002). As for the initial stress in the DMWs, isotropic stress of 170 kPa was given by considering the measured vertical pressure between the raft and the DMWs. The initial shear modulus was determined by the calibration analysis for the records of the 2011 off Pacific Coast Tohoku Earthquake (Shigeno et al., 2017). The strength and the properties of the stabilized soils are listed in Table 1. The parameters of the Namikawa model were referred to Namikawa et al. 2006 and listed in Table 2.

Table 1. Parameters of stabilized soil related to strength.

Compressive strength	F_c	MPa	2.6
Tensile strength	$0.2F_c$	kPa	520
Cohesion	$0.3F_c$	kPa	780
Friction angle	ϕ	degree	30
Poisson's ration	ν		0.26
Density	ρ	t/m^3	2.0
Initial shear modulus	G_0	MPa	500

Table 2. Parameters for Namikawa model.

Hardening parameter	α		0.9
Hardening parameter	e_y		0.0001
Fracture energy	G_f	N/m	96.0
Softening parameter for shear	e_r		0.4
Dilatancy coefficient	D_c		0.0
Localization size	l_m	mm	1000
Characteristics length	l_c	mm	0.6

4 RESULTS

The case without DMWs was also analysed to clarify their effect. Figure 5(a) shows the profiles of the peak acceleration at the center of the superstructure and the raft together with those of the ground at point A (Fig. 2). The result of the soil column model is also shown as 'far field', and the PGA at the surface is 296 gal. Comparing among the cases, the acceleration is slightly reduced by the raft and the DMWs. Figure 5(b) shows the profiles of the peak displacement that is relative to GL -49.9 m. The deformation beneath the raft is reduced by the grid-form DMWs, and this affects the sectional force of the piles.

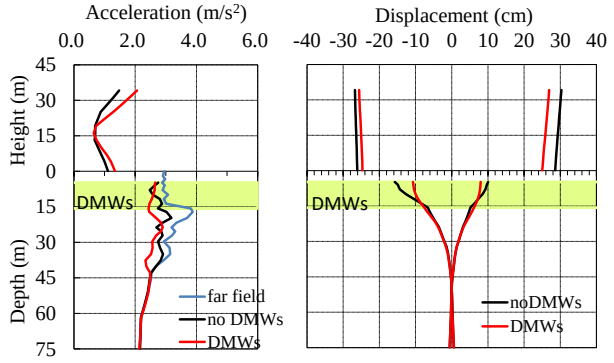

(a) Acceleration (b) Relative displacement

Fig. 5. Peak response profile of superstructure at center and ground at point A.

Figure 6 illustrates the extent of tensile failure in the DMWs during the earthquake in two different diagonally top views. Elements are colored according to the number of Gauss points where the induced stress reaches the initial tensile strength. Number of Gauss points is 8 in each element, and then the maximum value is 8. The tensile failure is seen mostly in the lower part of the longitudinal walls to the shaking direction, and this is due to shear deformation. In the most of the upper part of the walls, tensile failure is not seen because the deformation is restricted by the raft. In the transverse walls, some elements at the bottom of grid crossing corners fail clearly due to bending.

Figure 7 shows the tensile strength of the each element at the final time step. As shown in the figure, some elements totally lose their tensile strength. However the majority of the elements keep the high tensile strength, even though the stress of the some of them reaches the tensile strength as shown in the Fig. 6.

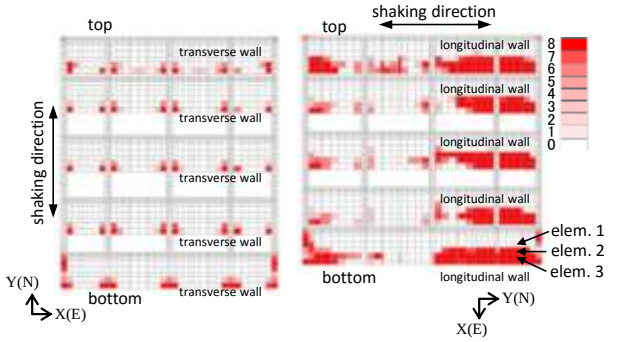

Fig. 6. Contour map of tensile failure Gauss points in DMWs (2 different diagonally top views).

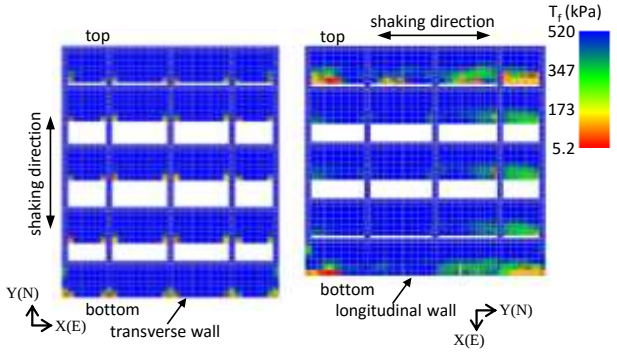

Fig. 7. Contour map of residual tensile strength at the final step (2 different diagonally top views).

Figure 8 shows the time histories of the maximum principal stress, and the tensile strength of the elements shown in Fig. 6. The red dot line is the initial tensile strength σ_{t0} = 520 kPa. In element 1, which is upper part of the DMWs, the stress does not reach σ_{t0}. Then, the softening does not occur. In element 2, the stress reaches σ_{t0}, and then the softening occurs. However the degradation rate is as small as 8%. This point keeps the high tensile strength even though tensile failure occurs. In element 3, the stress reaches σ_{t0} and the tensile strength is almost lost. These results show the colored regions in Fig. 6 do not mean the regions where the strength is totally degraded. It is important to notice that the elements have different residual tensile strength, even though they specify the same color in Fig. 6.

Figure 9 shows the profiles of the peak bending moment in piles 5B and 7B showed in Fig. 3. The peak value near the pile head in the case with DMWs is remarkably smaller than those in the case without DMWs. In the case with DMWs, the deformation of the soil enclosed by the DMWs is small and results in a small bending moment near the pile head. However, the moment at the bottom of the DMWs is large, because the curvature of displacement becomes large due to the

high rigidity of the DMWs. On the other hand, in the case without DMWs, the peak deformation near the pile head is large and asymmetric. This results in the large and asymmetric bending moment at the pile head. These results show the same tendency as the case without softening (Yamashita et al. 2018).

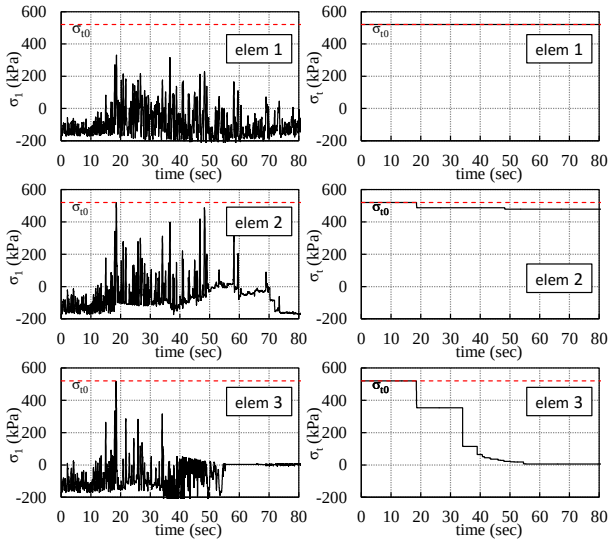

Fig. 8. Time histories of tensile stress and tensile strength of DMWs (element No. is in fig. 6).

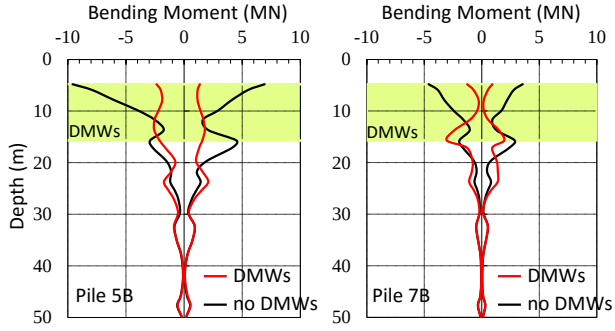

Fig. 9. Profiles of peak bending moment of piles.

Figure 10 shows the relationship between the axial force and the bending moment of Piles 5B and 7B, together with the design interaction curves of the steel pipe–concrete composite (SC) pile which is used in the top portion at 12 m. The axial force is the sum of the statically measured pile head load and the analytical dynamic increment force, and the bending moment is the maximum value along the SC pile. The results show that the bending moment in the case with DMWs is below the allowable criterion. In contrast, the bending moments in the case without DMWs are close to the ultimate criterion. Hence, the grid-form DMWs are quite effective at reducing pile bending moment to an acceptable level, although the induced stress in the stabilized soil partially reaches the tensile strength and softens under the strong earthquake load. This indicates that the grid-form DMWs can be designed more rationally by the performance-based design method in which a partial failure of the DMWs is accepted.

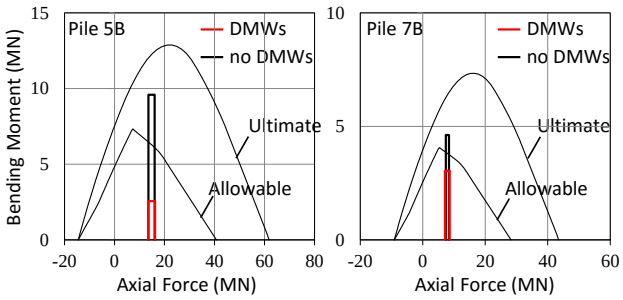

Fig. 10. Calculated maximum moment along pile and design N–M interaction curves of SC piles.

5 CONCLUSION

Seismic response analysis of a piled raft foundation with grid-form DMWs using the three dimensional nonlinear finite element model under a strong earthquake load is carried out considering after peak softening of the DMWs. As a result, the induced stress reaches the tensile strength and the softening occurs in some parts of the DMWs. However the majority parts of the DMWs keep the high tensile strength, and this results in keeping their effect on reducing sectional force of the piles to an acceptable level.

REFERENCES

Building Center of Japan. (2002). Specification for design and quality control of cement treated soil (in Japanese).

Namikawa, T. and Koseki, J. (2006). Experimental determination of softening relations for cement-treated sand, soils & foundations, Vol.46, No.4, 491-504.

Namikawa, T. and Mihira, S. (2007). Elasto-plastic model for cement-treated sand, Int. J. Numer. Anal. Meth. Geomech., Vol. 31, 71-107.

Shigeno, Y., Yamashita, K., Hamada, J. and Nakamura, N. (2017). Numerical evaluation of seismic performance of piled raft with grid-form DMWs under large earthquake loads, Design and analysis of pile raft foundations - 2017, Tamkang University Press, 109-127.

Shiomi, T., Shigeno, Y. and Zienkiewicz, O. C., (1993). Numerical prediction for model No. 1., Verification of Numerical Procedures for the Analysis of Soil Liquefaction Problems, Balkema, 213-219.

Tsujino, S., Yoshida, N. and Yasuda, S. (1994). A simplified practical stress-strain model in multi-dimensional analysis, Proc. Int. Symposium. on Pre-failure Deformation Characteristics of Geomaterials, Sapporo, Japan, 463-468.

Yamashita, K., Hamada, J., Onimaru, S. and Higashino, M. (2012). Seismic behavior of piled raft with ground improvement supporting a base-isolated building on soft ground in Tokyo, Soils & Foundations, Vol. 52(5), 1000–1015.

Yamashita, K., Hamada, J. and Tanikawa, T. (2016). Static and seismic performance of a friction piled combined with grid-form deep mixing walls in soft ground, Soils & Foundations, Vol. 56(3), 559-573.

Yamashita, K., Shigeno, Y. Hamada, J. and Chang, D. W. (2018). Seismic response analysis of piled raft with grid-form deep mixing walls under strong earthquakes with performance-based design concerns, Soils & Foundations, Vol. 58(1), 65-84.